

Desilylation of Substituted Polyacetylenes by Nanoparticles

Scott Matteucci,[†] Elizabeth Van Wagner,[†] Benny D. Freeman,^{*,†} Steve Swinnea,[†] Toshikazu Sakaguchi,[‡] and Toshio Masuda[‡]

Department of Chemical Engineering, The University of Texas at Austin, 10100 Burnet Road, Building 133, Austin, Texas 78758, and Department of Polymer Chemistry, Graduate School of Engineering, Kyoto University, Kyoto 606-8501, Japan

Received October 20, 2006; Revised Manuscript Received February 16, 2007

ABSTRACT: Magnesium oxide (MgO) nanoparticles were dispersed via solution processing in trimethylsilyl-substituted polyacetylenes to form polymer nanocomposites. In the presence of these particles, the polymers, poly(1-trimethylsilyl-1-propyne) (PTMSP) and poly[1-phenyl-2-[*p*-(trimethylsilyl)phenyl]acetylene] (PTMSDPA), were partially desilylated. Some PTMSDPA/MgO nanocomposites were insoluble in common solvents (e.g., toluene or chloroform), and the solubility characteristics depended on particle loading and preparation conditions. When possible, the reaction products were characterized using XPS, FTIR, and NMR. Small molecule model compounds were also used to study the reaction of trimethylsilyl groups with MgO nanoparticles. The CO₂ permeability in these nanoparticle-filled films was over 6 times higher than in the analogous unfilled polymers. This phenomenon may provide a route for preparing highly permeable, chemically stable membranes for gas separations.

Introduction

Recent membrane-based gas separation applications have focused on the removal of organic vapors from mixtures with permanent gases.^{1–4} These separations include, for example, the removal of higher hydrocarbons from natural gas and hydrogen mining from mixtures with hydrocarbons in refineries.² As a class of materials, substituted polyacetylenes exhibit high permeability and high selectivity in such applications.⁵ For example, poly(1-trimethylsilyl-1-propyne) (PTMSP) (cf. Table 1) has an *n*-C₄H₁₀ permeability of 80 000 barrer (35 °C, Δ*p* = 1.1 atm) and an *n*-C₄H₁₀/CH₄ selectivity of 48 when exposed to a 98 mol % CH₄/2 mol % *n*-C₄H₁₀ gas mixture (25 °C, Δ*p* = 11.2 atm).⁶ Similarly, poly(1-phenyl-2-[*p*-(trimethylsilyl)phenyl]acetylene) (PTMSDPA) has a pure gas *n*-butane permeability of 20 000 barrer and a pure gas CH₄ permeability of 1600 barrer (25 °C, Δ*p* = 0.6 atm for *n*-C₄H₁₀ and 3.4 atm for CH₄).⁷ The *n*-C₄H₁₀/CH₄ separation has been used as a marker for the removal of higher hydrocarbons from natural gas, which is a separation required to adjust the heating value and dew point of natural gas to pipeline specifications.^{1,2} This separation is currently performed using energy-intensive condensation processes.² Membranes that are sufficiently permeable to higher hydrocarbons and highly selective for higher hydrocarbons over CH₄ could be of interest for this separation.¹

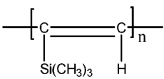
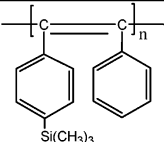
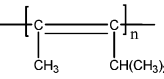
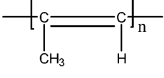
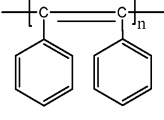
The addition of impermeable, surface-treated fumed silica (FS) nanoparticles increases the permeability of some substituted polyacetylenes.^{8–10} For example, the addition of 45 wt % FS increases *n*-C₄H₁₀ permeability of poly(4-methyl-2-pentyne) (PMP) (from 9200 to 27 000 barrer) and mixed gas *n*-C₄H₁₀/CH₄ selectivity (from 13 to 21) (25 °C, Δ*p* = 10.2 atm).⁹ From a gas transport perspective, substituted polyacetylenes exhibit the best combinations of permeation and selectivity of all known polymers for selective removal of larger organic vapors from mixtures with smaller permanent gases, and nanoparticles can enhance their separation properties.^{11,12}

* Corresponding author: Tel +01-512-232-2803; Fax +01-512-232-2807; e-mail freeman@che.utexas.edu.

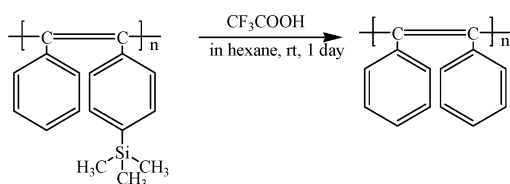
[†] The University of Texas at Austin.

[‡] Kyoto University.

Table 1. Structures of Selected Polyacetylenes

poly(1-trimethylsilyl-1-propyne) [PTMSP]	
poly(1-phenyl-2-[<i>p</i> -(trimethylsilyl)phenyl]acetylene) [PTMSDPA]	
poly(4-methyl-2-pentyne) [PMP]	
poly(methylacetylene)	
poly(diphenylacetylene) [PDPA]	

However, a limitation of substituted polyacetylenes as viable membrane materials is their high solubility in higher hydrocarbons or aromatics such as toluene; such compounds could be present in the gas streams that would be candidates for separation using such polymers, thereby limiting the utility of these materials for vapor separations.^{2,13,14} PTMSP, PTMSDPA, and poly(methylacetylene) (cf. Table 1) dissolve readily in hydrocarbon solvents such as toluene, hexane, and benzene.^{9,15–17} However, many materials from the same family of polymers, such as poly(acetylene) and poly(diphenylacetylene) (PDPA), are insoluble in organic solvents.^{17,18} Because of the insolubility of PDPA in organic solvents, films and membranes of this material have only been prepared via desilylation of a soluble

Scheme 1. PTMSDPA Desilylation Reaction with Trifluoroacetic Acid Treatment²⁰

substituted precursor, such as PTMSDPA.¹⁹ The desilylation was accomplished by exposing a PTMSDPA film to a mixture of hexane and trifluoroacetic acid for 24 h at room temperature, as presented in Scheme 1.²⁰ After neutralizing the excess acid with triethylamine, impurities were removed by immersing the film in methanol for 5 h and then washing it with methanol.²⁰ Desilylation, while imparting chemical stability, was accompanied by a marked diminution in permeability.^{19,20} For example, CO₂ permeability in PTMSDPA is 4000 barrer, but it is only 1500 barrer in desilylated PTMSDPA (i.e., PDPA) (35 °C, $\Delta p = 10.2$ atm).²¹

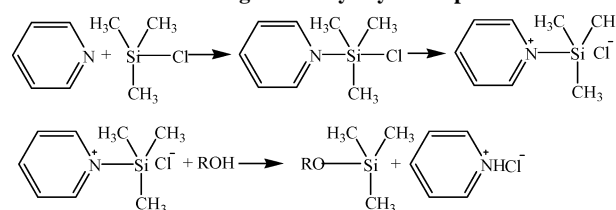
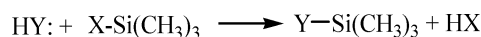
The purpose of this study is to demonstrate the ability of reactive nanoparticles to alter chemical stability and light gas permeation properties in polymeric membranes. We report partial desilylation of highly soluble PTMSDPA to insoluble PDPA resulting from dispersing magnesium oxide (MgO) nanoparticles in PTMSDPA by solution blending and film casting. We report desilylation of PTMSP by the same process. The reaction products were characterized using X-ray photoelectron spectroscopy (XPS), Fourier transform infrared spectroscopy (FTIR), and nuclear magnetic resonance (NMR) spectroscopy. Low molar mass model compounds were used to further study this desilylation reaction in the presence of nanoparticles. CO₂ and CH₄ permeabilities are reported for PTMSDPA/MgO nanocomposite films for comparison with permeation results reported for substituted polyacetylene films prepared via desilylation using trifluoroacetic acid.

Background

Trimethylsilyl Chemistry. Polymers containing trimethylsilyl (TMS) groups often exhibit higher gas and vapor permeability than their analogues without TMS groups.^{4,5} For example, materials such as PTMSDPA and poly(vinyltrimethylsilane) have higher diffusivity and permeability coefficients than their non-TMS-containing analogues.^{21–23} The diffusivity enhancement has been attributed to disruption of chain packing by bulky TMS groups.^{21–23}

The TMS group has several attributes which are relevant to the study of polymer desilylation by metal oxide nanoparticles. Silicon atoms have 3d orbitals available for bonding, and they allow silicon to form transition states with pentavalent bonds.²⁴ The 3d bond orbital conjugates effectively with adjacent p orbitals such as lone pair electrons on oxygen, nitrogen, and sulfur or with π -bonded carbon.²⁴ The (d–p) π bonding has been credited with increasing the reactivity of Si–Y bonds relative to C–Y bonds.²⁵ These composite characteristics render TMS groups chemically reactive under certain circumstances.²⁴

Teraguchi and Masuda reported the use of trifluoroacetic acid to desilylate PTMSDPA, as shown in Scheme 1.²⁰ FTIR indicated complete PTMSDPA conversion to PDPA based upon the disappearance of peaks ascribed to TMS groups in PTMSDPA (i.e., 1250 cm^{–1} for SiC–H as well as 1119, 855, and 812 cm^{–1} for Si–CH₃).²⁰ The CO₂ permeability of the resulting PDPA membrane is 1500 barrer as compared to 4000 barrer for PTMSDPA.²¹ The CO₂/CH₄ selectivity was the same for both PTMSDPA and PDPA.²¹

Scheme 2. Reaction between Basic Compounds and Compounds Containing Trimethylsilyl Groups²⁶**Scheme 3. Generic Desilylation Reaction Mechanism for Basic Molecules²⁴**

Basic alcohols desilylate small organic molecules containing TMS groups.²⁴ For instance, Henglein and Scheinost report the desilylation of small molecules, as shown in Scheme 2,²⁶ where R represents either glucose or pectin. In the second step, the positive charge on the nitrogen atom is stabilized by conjugation with the pyridine ring. Such stabilization by conjugation is reported to be important for this reaction.²⁴ In general, basic alcohol lone pair electrons form a p–d bond with the silicon atom of trimethylsilyl groups.²⁴ Desilylation is most probable when the TMS donor is less basic than the acceptor and when the donor is conjugated to stabilize the p–d bond. The desilylation reaction mechanism of basic alcohols and organic compounds containing TMS groups is presented in Scheme 3,²⁴ where Y is a TMS acceptor and X is a TMS donor.

Gas Transport in Polymers. The permeability of gas A, P_A , through a film of thickness l is:^{4,27}

$$P_A \equiv \frac{N_A l}{(p_2 - p_1)} \quad (1)$$

where N_A is the steady-state gas flux through the film; p_2 and p_1 are the feed and permeate partial pressures of gas A, respectively. If Fick's law is obeyed and the downstream pressure, p_1 , is much lower than the upstream pressure, p_2 , the permeability is often expressed as:²⁷

$$P_A = D_A S_A \quad (2)$$

where D_A is the effective, concentration-averaged diffusivity. The effective solubility coefficient, S_A , is defined as C_2/p_2 , where C_2 is the concentration of gas A in the polymer at the upstream face of the film. The ability of a polymer to separate two components is often characterized by the ideal selectivity, $\alpha_{A/B}$, which is the ratio of permeabilities of the two components.^{4,27} Using eq 2, the ideal selectivity may be expressed as a product of D_A/D_B , the diffusivity selectivity, and S_A/S_B , the solubility selectivity:^{4,27}

$$\alpha_{A/B} \equiv \frac{P_A}{P_B} = \frac{D_A S_A}{D_B S_B} \quad (3)$$

Diffusivity selectivity depends primarily on the relative sizes of the penetrant molecules and the size-sieving ability of the polymer, which can be a strong function of free volume in the polymer matrix.^{4,28} Solubility selectivity is controlled primarily by the relative condensability of the penetrants and the relative affinity of the penetrants for the polymer matrix.^{4,28}

Permeability in heterogeneous films is a strong function of the dispersed phase geometry, concentration, and permeability.^{29,30} Traditionally, adding an impermeable dispersed phase (e.g., nanoparticles) to a polymeric matrix reduces overall

permeability.³¹ The permeability reduction is attributed to an increase in penetrant diffusion pathway tortuosity (which decreases effective diffusivity) and a loss in polymer volume available for sorption and diffusion.⁸ However, when substituted polyacetylenes are filled with nanoscale fillers, such as fumed silica, the permeability of the resulting nanocomposites can increase with increasing particle loading.^{6,8} The elevated permeability for nanoparticle filled substituted polyacetylene films has been attributed to nanoparticle-induced increases in fractional free volume.^{6,8,32}

Experimental Section

Nanoparticles. MgO Plus (Nanoscale, Manhattan, KS) was used in this study. According to the supplier, these MgO nanoparticles have a specific gravity of 3.58 g/cm³ and a BET surface area between 600 and 680 m²/g. The resulting average equivalent spherical particle diameter is 2.6 nm, where equivalent spherical particle diameter is defined as 6/(surface area × density). Samples are reported to be spherical, and the metal composition is 99.2% pure Mg, with the remainder being trace impurities. Such MgO aerogels readily deagglomerate in organic solvents such as toluene.³³

Polymers. Poly(1-trimethylsilyl-1-propyne) was kindly supplied by Air Products and Chemicals, Inc. (Allentown, PA), and poly-(1-phenyl-2-[*p*-(trimethylsilyl)phenyl]acetylene) was prepared as described elsewhere.¹⁹ Both polymers were high molar mass materials that readily form films from solution in toluene.

PTMSP Nanocomposite Film Preparation. Glassware used in this study was cleaned and dried at 80 °C overnight. Unless otherwise noted, the glassware was allowed to cool to room temperature at ambient conditions prior to being moved to a N₂-blanketed glovebox.

PTMSP was added to 99.8% anhydrous toluene from Sigma-Aldrich (St. Louis, MO) (1.5 g of PTMSP per 100 mL of toluene) and stirred using a magnetic stir bar until the polymer dissolved. Nanoparticles were added to the solution to prepare a final dry film having a target filler volume fraction, ϕ_F^N , which was calculated as follows:

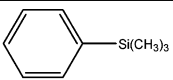
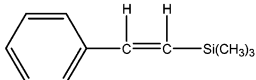
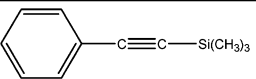
$$\phi_F^N = \frac{W_F/\rho_F}{W_P/\rho_P + W_F/\rho_F} \quad (4)$$

where W_F and W_P are the masses of filler and polymer in the sample, respectively; ρ_F and ρ_P are the densities of pure filler (3.58 g/cm³) and pure polymer (0.75 g/cm³),⁵ respectively. This definition of filler volume fraction is the so-called nominal volume fraction. It provides a convenient measure of the relative proportion of filler in the polymer. If the polymer or particle density is influenced by the nanocomposite preparation process, then this value will be different from the true filler volume fraction. This issue is discussed in more detail elsewhere.³⁴

The particle-filled solution was mixed at 15 000 rpm for at least 5 min using a Waring handheld high-speed blender (Stamford, CT). The particle-filled solution was then allowed to mix overnight at ambient conditions using a magnetic stir bar. Afterward, the solution was poured onto a clean, dry, level glass casting plate and allowed to dry at ambient conditions until the toluene had completely evaporated, which usually required about 2 days. All PTMSP sample preparation steps involving particles were conducted in a glovebox under a N₂ blanket, and a relative humidity of 0.0 (as determined by a Tescom hydrometer (Elk River, MN)) was maintained at all times. The N₂ blanket was used to minimize the exposure of the particles to water, since MgO particles can react with water.³⁵

PTMSDPA Nanocomposite Film Preparation. PTMSDPA was dissolved in toluene (1 g of PTMSDPA in 100 mL of 99.8% anhydrous toluene). The solution was stirred for 24 h at ambient conditions using a magnetic stir bar. Afterward, the solution was stirred for 4 h at a prescribed temperature (i.e., -10, 0, and 23 °C) to explore the influence of mixing temperature on the extent of

Table 2. Model Compounds Considered

Trimethyl(phenyl)silane [TMPS]	
1-phenyl-2-(trimethylsilyl)-ethylene [PhTMSE]	
1-phenyl-2-(trimethylsilyl)-acetylene [PhTMSA]	

reaction between the particles and polymer. MgO nanoparticles were then added to the solution, and it was shaken to disperse the nanoparticles. The particle-filled solution was stirred for a fixed amount of time using a magnetic stir bar at the prescribed temperature. The solution was then poured onto a clean, dry, level glass casting plate in a fume hood and covered with a Petri dish to slow evaporation. Films were cast at room temperature (~23 °C) and generally required 2 days for complete solvent removal.

MgO-Treated Model Compounds. The chemical structures of the low molar mass model compounds used in this study are presented in Table 2, and all of the compounds were obtained from Sigma-Aldrich (St. Louis, MO). 0.39 g of 1-phenyl-2-(trimethylsilyl)acetylene (PhTMSA) (cf. Table 2), 0.39 g of 1-phenyl-2-(trimethylsilyl)ethylene (PhTMSE), and 0.35 g of trimethyl(phenyl)silane (TMPS) were each dissolved individually in 10 g of *d*-benzene from Fisher Scientific (Hampton, NH). These masses of model compounds correspond to the TMS molar concentration in 0.25 g of PTMSP dissolved in 10 g of *d*-benzene, which was the sample concentration used for the NMR experiments described below. After mixing for 1 h using a magnetic stir bar, MgO nanoparticles were added to the solution. The amount of MgO added to the solution was characterized by Γ , which is the ratio of moles of TMS per gram of MgO. Γ was calculated as follows:

$$\Gamma = \frac{m_{MC}}{M_{MC}m_{MgO}} \quad (5)$$

where M_{MC} is the molar mass of the model compound (174 for PhTMSA, 176 for PhTMSE, and 150 for TMPS), and m_{MC} and m_{MgO} are the masses of the model compound and MgO added to the solution, respectively. To vary Γ , m_{MC} is held constant and m_{MgO} was changed. The resulting solution was mixed overnight at ambient conditions using a magnetic stir bar.

Wide-Angle X-ray Diffraction (WAXD). Wide-angle X-ray diffraction was performed using a Scintag X1 theta-theta diffractometer. Cu K α radiation with a wavelength of 1.54 Å was used. The power settings were 45 kV and 40 mA. The software used for data processing was Jade v. 7.5 from Materials Data Inc., Livermore, CA. The powder diffraction database used for comparing the experimental data to known powder diffraction patterns was PDF-2 Release 2004 from the International Centre for Diffraction Data, Newton Square, PA.

Fourier Transform Infrared Spectroscopy (FTIR). Polymer and polymer composite samples were examined using FTIR (Thermo Nicolet Nexus 470, Madison, WI) with an ATR Smart Avatar attachment (Thermo Nicolet Nexus, Madison, WI). The crystal was cleaned with isopropyl alcohol prior to collecting the background. Whenever possible, samples were tested immediately after removal from the glovebox. Model compounds were prepared in KBr (Sigma-Aldrich) pellet samples and examined using transmission FTIR (Thermo Nicolet Nexus 470, Madison, WI).

Toluene or Chloroform Solubility Test. PTMSDPA, PTMSP, and polymethylacetylene (i.e., desilylated PTMSP) are highly soluble in toluene or chloroform.²⁰ In contrast, desilylated PTMS-

DPA (i.e., PDPA) is insoluble in these solvents.²⁰ So, extracting PTMSDPA–MgO nanocomposites in toluene or chloroform and monitoring the solids content of the sample provides an indication of the influence of the nanoparticles on nanocomposite solubility. Nanoparticle-filled PTMSDPA films weighing ~0.1 g were placed in sealed containers with 50 mL of either toluene (Sigma-Aldrich) or chloroform (Sigma-Aldrich). This ratio of polymer to solvent is well below the solubility limit of PTMSDPA in either solvent.²⁰ The films were extracted for at least 2 weeks at ambient conditions in solvent. After 2 weeks, the films were removed from solvent either using tweezers, if the film had sufficient mechanical strength, or the films were removed by filtering the solvent from the solids using a filter attached to a vacuum. Samples that required filtering were either in a gel-like state or appeared to be fragile polymer films. After removal from solvent, samples were dried for 2 days in a fume hood. The percent weight loss, ΔM , was estimated as follows:

$$\Delta M = \left(1 - \frac{M_s}{M_0}\right) \times 100 \quad (6)$$

where M_0 and M_s are the weights of the dry nanocomposite sample before and after extraction in toluene or chloroform, respectively. This calculation does not distinguish between polymer and/or particle extraction from the film. Therefore, it provides a qualitative demonstration of the effects of mixing time, solution temperature, and particle loading on the chemical stability of PTMSDPA nanocomposites in solvents that are quite effective for dissolving the native polymer and for dispersing the particles.

X-ray Photoelectron Spectroscopy (XPS). An XPS system equipped with a monochromatic Al $K\alpha_{1,2}$ X-ray source (PHI 5700, Physical Electronics Inc., Chanhassen, MN) was used to examine films for evidence of reaction. Operating conditions were 1×10^{-9} Torr chamber pressure and 14 kV, 250 W for the Al X-ray source.

Proton and Carbon Nuclear Magnetic Resonance (^1H NMR and ^{13}C NMR). ^1H and ^{13}C solution NMR spectra were observed on an RT Quad Probe Unity +300 (Varian, Palo Alto, CA). Proton NMR experiments were conducted at 500 MHz, and ^{13}C NMR experiments were conducted at 125 MHz. Nanocomposite films were dissolved in d-benzene such that each sample contained 0.25 g of polymer, regardless of particle volume fraction. This procedure assured that all NMR samples would have sufficient polymer present to obtain meaningful data. Model compounds were added directly to d-benzene containing MgO and allowed to stir overnight at ambient conditions prior to testing. All samples were referenced to the solvent, d-benzene. ^1H NMR experiments were conducted over 1 h. ^{13}C NMR experiments were taken over a period of at least 16 h to improve resolution.

Permeability. Pure gas permeability was determined using a constant pressure/variable volume apparatus.³⁶ Films were 150–300 μm thick. Samples were masked with aluminum tape. After a film was placed in the permeation cell, it was exposed to the test gas at 3.4 atm upstream pressure for at least 30 min to ensure that steady state was established. Gas permeability (cm^3 (STP) $\text{cm}/(\text{cm}^2 \text{ s cmHg})$) was calculated from the steady-state permeate flow rate through a bubble flow meter according to³⁷

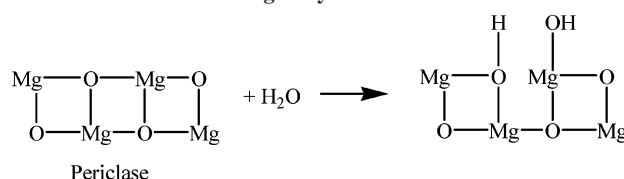
$$P_A = \frac{273p_{\text{atm}}}{76T} \frac{l}{A(p_2 - p_1)} \frac{dV}{dt} \quad (7)$$

where dV/dt is the permeate volumetric flow rate (cm^3/s), l is the film thickness (cm), p_2 is the upstream absolute pressure (cmHg), p_1 is the downstream absolute pressure (cmHg), p_{atm} is atmospheric absolute pressure (cmHg), A is the area of the film available for transport (cm^2), and T is absolute temperature (K). All experiments were performed at atmospheric downstream pressure (76 cmHg).

Results and Discussion

Reaction of MgO Nanoparticles with Water. A reaction was observed between MgO and the polymers under study (i.e.,

Scheme 4. MgO Hydration Reaction⁴⁰



PTMSDPA and PTMSP). As explained in more detail below, this reaction resulted in removal of at least some TMS groups from the polymer. The first step in the desilylation reaction mechanism is believed to be reaction of MgO (i.e., periclase) with adventitious water to form brucite, the mineral form of magnesium hydroxide ($-\text{MgOH}$), as shown in Scheme 4.³⁵ In this way, the particles become partially functionalized with $-\text{MgOH}$ groups.^{38,39} Since the brucite formed in this reaction is a part of the overall nanoparticle structure (e.g., $-\text{Mg}-\text{O}-\text{MgOH}$)^{35,40} and does not disassociate in solution,^{35,41} it is labeled as $-\text{MgOH}$ rather than $\text{Mg}(\text{OH})_2$.

As shown in Figure 1a, the WAXD data indicated that the particle structure prior to mixing with the polymer solution was predominantly periclase, which is the crystalline structure of MgO.⁴⁰ There was no discernible evidence of brucite in the WAXD spectrum of the neat particles even after exposure to ambient conditions for 1 week. When the MgO nanoparticles were soaked in deionized water with a resistance of 18.2 $\text{M}\Omega \cdot \text{cm}$ prepared by a Milli-Q plus TOC (Millipore, Billerica, MA) for 48 h, the particles converted to brucite, as shown in Figure 1a.

The spectrum of PTMSP filled with 0.2 volume fraction MgO particles exhibits peaks indicating the presence of both periclase and brucite (cf. nanocomposite 1 in Figure 1b). That is, $-\text{MgOH}$ functional groups were present in the nanocomposite but not in the particles prior to being mixed with the polymer solution. The brucite peaks did appear in the WAXD spectrum of MgO particles soaked in 99.8% anhydrous toluene for 2 days and allowed to dry in a fume hood for 2 days, so the partial conversion of periclase to brucite did not require the presence of PTMSP in the solution. Thus, using the protocol described in the Experimental Section, a reaction between MgO and water takes place. Although the nanocomposite solution and films were prepared in a dry glovebox, it seems likely that there were traces of water adsorbed on glassware or in the solvent with which the particles could have reacted.

A more rigorous drying procedure suppresses conversion of periclase to brucite. Adventitious water introduced from the glassware can be suppressed by drying the glassware at 80 $^\circ\text{C}$ overnight and placing the warm glassware into the N_2 -blanketed glovebox. Using anhydrous toluene from Acros Organics (Geel, Belgium) containing less than 50 ppm water reduces another potential source of moisture. Nanocomposite 2 in Figure 1b was prepared under these conditions, and it exhibited no peaks associated with brucite in WAXD. The peak at around 9.5 $^\circ$ is associated with PTMSP (cf. Figure 1b), and it is consistent with the PTMSP WAXD spectrum in the literature.¹⁵ The results discussed below were obtained using the protocol described in the Experimental Section, that is, using the sample preparation method that results in the conversion of some periclase to brucite.

The spectrum of MgO-filled PTMSDPA, when the particles are mixed with the polymer at low temperatures, did not exhibit peaks associated with brucite (cf. nanocomposite 3 in Figure 1c). The spectrum of PTMSDPA exhibited peaks at 6.3 $^\circ$ and 14.5 $^\circ$ as presented in Figure 1c, which is consistent with the spectrum reported in the literature.¹⁶ As discussed in more detail

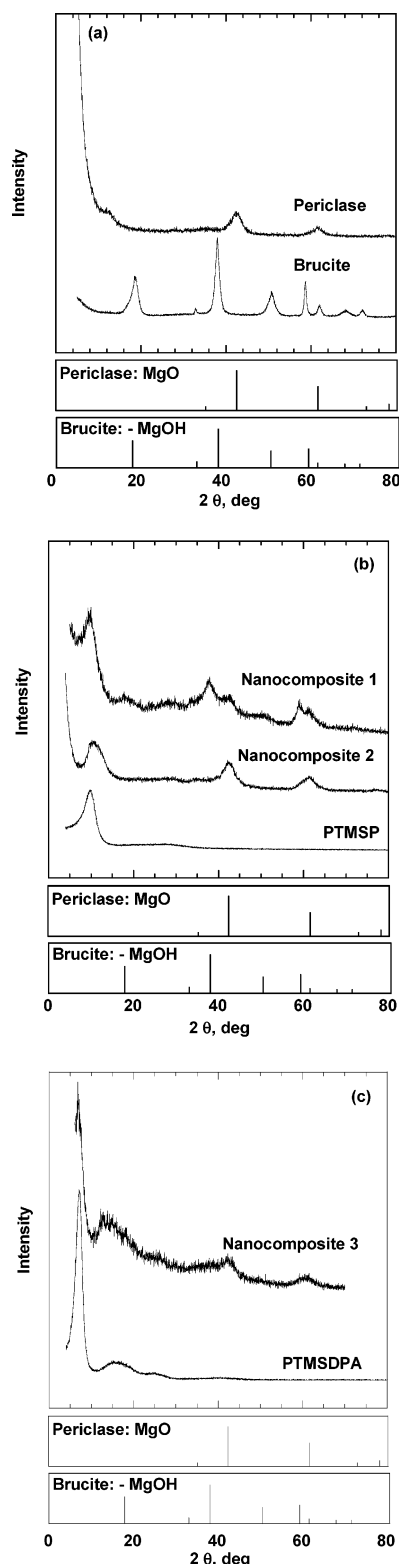
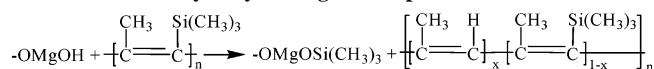


Figure 1. WAXD patterns for (a) neat MgO nanoparticles exposed to ambient conditions for 1 week prior to testing (periclase) and soaked in deionized water for 48 h and dried for 48 h in a fumed hood (brucite); (b) 0.2 volume fraction MgO in PTMSP after 2 days of mixing at 23 °C (nanocomposite 1), prepared with dry toluene and dry glassware after 2 days of mixing at 23 °C and cast in a dry glovebox (nanocomposite 2), and unfilled PTMSP; and (c) 0.2 volume fraction MgO in PTMSDPA after 5 days of mixing at -10 °C (nanocomposite 3) and unfilled PTMSDPA. The boxes below each graph present 2θ peak locations and intensities associated with periclase and brucite crystal structures from the powder diffraction database, PDF-2 Release 2004 from the International Centre for Diffraction Data, Newton Square, PA. The WAXD spectra were shifted vertically for easier viewing.

Scheme 5. Proposed PTMSP Desilylation Reaction by Hydrolyzed MgO Nanoparticles



below, the absence of brucite in the WAXD spectrum of this sample may result from the consumption of most of the available -MgOH groups by the desilylation reaction.

Desilylation of PTMSP. The proposed reaction mechanism of PTMSP with brucite alcohol groups is presented in Scheme 5. The alcohol groups on magnesium hydroxide are electron-rich and basic,⁴³ which favors their participation in reactions of the type shown in Scheme 3. The PTMSP backbone could serve as a TMS donor. Also, the polymer backbone is somewhat conjugated,⁵ which allows p-d bond stabilization, and this effect also favors reactions of the type illustrated in Schemes 3 and 5.²⁴ From Scheme 3, Y would represent MgO- and X would represent the PTMSP backbone. The lone pair electrons on -Mg-OH groups may form a p-d bond with silicon, which would be stabilized by conjugation with the PTMSP backbone.

ATR FTIR spectra of pure MgO, pure PTMSP, and a nanocomposite film of PTMSP containing MgO are presented in Figure 2. The MgO nanoparticles did not exhibit any peaks between 675 and 4000 cm⁻¹, and this result is consistent with the literature.⁴⁴ The PTMSP spectrum exhibits a peak at 1540 cm⁻¹, which is attributed to carbon-carbon double bonds, as well as peaks at 1240, 820, and 740 cm⁻¹, which are attributed to SiC-H and Si-CH₃ bonds, respectively. These peaks and their assignments are consistent with those reported by Masuda et al.¹⁵ The spectrum for PTMSP/MgO films contains PTMSP peaks and several additional peaks. The MgO-Si peak at 1092 cm⁻¹ suggests that desilylation occurred.⁴⁵ Other differences between the spectra of the PTMSP and PTMSP/MgO samples were at 2300–2400 cm⁻¹ and at 1400–1550 cm⁻¹, consistent with physisorption⁴⁶ and chemisorption^{35,44} of CO₂ on MgO, respectively. CO₂ chemisorbed to MgO leads to the formation of -MgCO₃.^{35,44} Any differences in the peaks associated with physisorbed CO₂ (i.e., the peak at 2200–2400 cm⁻¹) can be attributed to differences in the background levels of CO₂ present when the background and sample scans were collected.

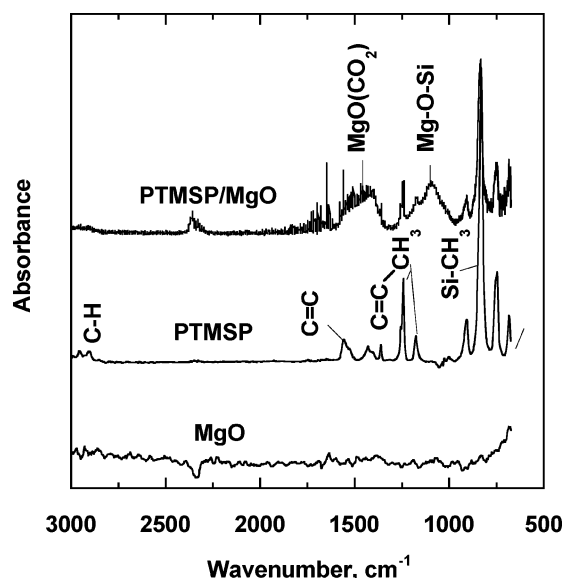


Figure 2. ATR FTIR of MgO, PTMSP, and PTMSP containing 0.2 volume fraction MgO. The PTMSP/MgO spectrum was shifted vertically for easier viewing. Peak assignments for PTMSP are from Masuda et al.¹⁵ Peak assignments for MgOH,³⁵ physisorbed CO₂,⁴⁶ chemisorbed CO₂ (i.e., MgO(CO₂)),^{35,44} and Mg-O-Si²⁴ are consistent with the literature.

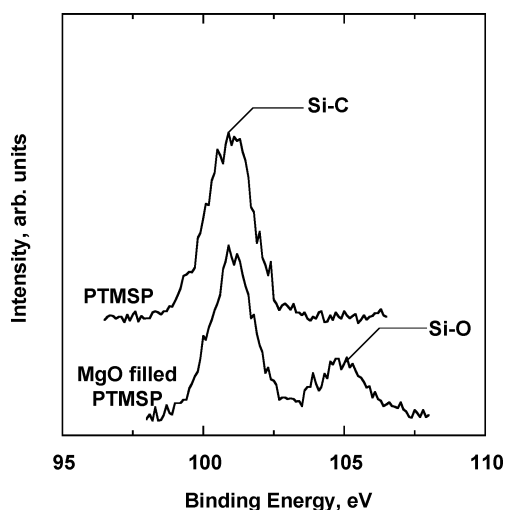


Figure 3. XPS of Si 2p orbital for PTMSP and PTMSP containing 0.2 volume fraction MgO.

Figure 3 presents XPS characterization of the silicon 2p orbital of PTMSP and a PTMSP/MgO nanocomposite. From these spectra, Si had bonds to two different elements in the nanocomposite sample, but not in the polymer. The peak at 101 eV corresponds to Si–C bonds,⁴⁷ and this peak is observed in both the PTMSP film and the PTMSP/MgO film. The peak at 105 eV is ascribed to the presence of Si–O bonds.⁴⁸ The particles provide the only oxygen source in the PTMSP/MgO film. The PTMSP provides the only source of Si in these materials since XPS did not detect Si in the neat MgO nanoparticles, as expected. Therefore, the XPS results corroborate the existence of Mg–O–Si bonds, which should be present if PTMSP were partially desilylated according to Scheme 5.

One advantage of using PTMSP in the desilylation studies is that the desilylated product, a copolymer of PTMSP and poly(methylacetylene), remains soluble in organic solvents, including d-benzene. This feature allows the reaction products to be characterized by solution NMR. ¹H NMR solution spectroscopy was conducted on PTMSP and PTMSP/MgO samples to characterize changes in the polymer structure due to the reaction, and the results are presented in Figure 4. As shown in Figure 4a, the ¹H NMR spectrum for PTMSP exhibited peaks at 0.8 and 2.1 ppm, and they are attributed to protons on the TMS methyl groups and the lone methyl group, respectively. These results are consistent with those reported by Masuda et al.¹⁵ As shown in Figure 4b, these peaks were also present in the ¹H NMR spectrum for the PTMSP nanocomposite. The peak at 0.8 ppm (i.e., protons on the TMS groups) in the nanocomposite indicates that the desilylation reaction did not proceed to completion. Also, a singlet peak was observed at 3.1 ppm in the PTMSP/MgO spectrum, and this peak is not observed in the spectrum of the polymer alone (cf. Figure 4a). Since PTMSP did not have a peak at 3.1 ppm, it is assigned to the olefinic proton produced by the desilylation reaction. The 3.1 ppm peak is at a different location than the olefinic proton peak value of 5.9 ppm reported for pure poly(methylacetylene).⁴⁹ However, the silylated constituents on the polymer chain may shift the olefinic proton peak to a lower value. The chemical shift of olefinic protons in polyacetylenes often varies widely depending on the secondary polymer structure.⁵⁰

Using the NMR data, the fractional desilylation, X_{TMS} (moles of TMS removed/mole of TMS in the polymer before desilyl-

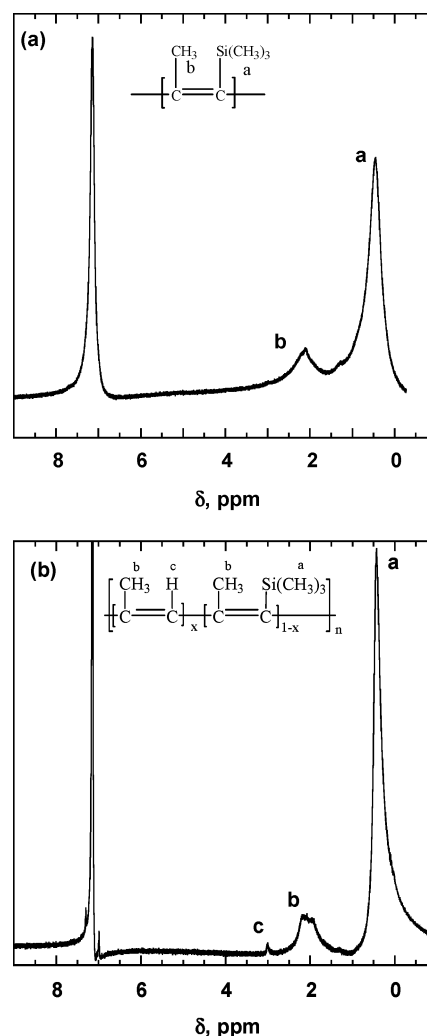


Figure 4. ¹H NMR of (a) PTMSP and (b) PTMSP containing 0.2 volume fraction MgO. The peak at 7.2 ppm is ascribed to the hydrogen atoms in the d-benzene solvent.

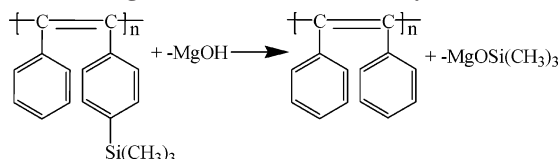
ation), can be estimated as follows:

$$X_{\text{TMS}} = \frac{I_c}{I_a + \frac{I_c}{9}} \times 100 \quad (8)$$

where I_a is the integral value of the TMS group of PTMSP at peak a and I_c is the proton integral value of the desilylated PTMSP olefinic proton peak c. In this case, I_a is divided by nine because there are nine hydrogen atoms on a TMS group, and they are replaced by one hydrogen when desilylation occurs. On the basis of eq 8 and the data in Figure 4b, 9% of the TMS groups were removed from the polymer due to contact with MgO according to the sample preparation protocol described earlier.

Desilylation of PTMSDPA. If the desilylation of PTMSDPA follows a similar mechanism to that of PTMSP, the reaction would proceed as indicated in Scheme 6. The phenyl groups may increase the conjugation of the PTMSDPA polymer backbone,^{16,20} which may, in turn, stabilize the MgOH–TMS bond more effectively than in PTMSP. PTMSDPA and nanocomposites containing 0.2 volume fraction MgO in PTMSDPA were examined by FTIR, and the results are presented in Figure 5. The PTMSDPA peaks at 1250 cm^{-1} (SiC–H) and at 1119, 855, and 812 cm^{-1} (Si–CH₃) are in agreement with the spectrum reported for PTMSDPA by Tsuchihara et al.¹⁶ and

Scheme 6. MgO-Induced PTMSDPA Desilylation Reaction



by Teraguchi and Masuda.^{16,20} The PTMSDPA/MgO film contained a new peak at 1092 cm^{-1} . This new peak is consistent with the peak at 1092 cm^{-1} in the PTMSP/MgO spectrum, and it is attributed to Mg—O—Si bonds formed as a result of the desilylation reaction shown in Scheme 6.

Like PDPA (i.e., desilylated PTMSDPA), the PTMSDPA/MgO samples were insoluble in d-benzene, so solution NMR studies could not be performed. Testing nanocomposite solubility in known solvents for PTMSDPA provides indirect evidence for the desilylation of PTMSDPA by MgO nanoparticles. As demonstrated below, the weight loss of PTMSDPA/MgO nanocomposites after extraction in toluene depends on MgO loading, PTMSDPA/MgO solution mixing time, and solution mixing temperature. Increasing MgO loading, while holding the other parameters constant, substantially decreased weight loss due to extracting the nanocomposite in toluene, as shown in Figure 6. Since PTMSDPA is soluble in toluene and the MgO particles are readily dispersed in toluene, if there were no interaction between the polymer and particles, the weight loss would be 100%, which is the result obtained in the absence of particles (i.e., 0 volume fraction MgO in Figure 6). On the other hand, if the polymer/particle film is completely insoluble in toluene, then the weight loss upon extraction in toluene would be 0%. This limit is achieved in samples containing 0.35 and 0.5 volume fraction nanoparticles. Similar insolubility results were found for PTMSDPA/MgO films in chloroform extraction experiments, and chloroform is another good solvent for PTMSDPA.²⁰

Similar behavior was observed with respect to the PTMSDPA/MgO solution mixing time. As shown in Figure 7, increasing mixing time generally decreased nanocomposite weight loss due to toluene extraction. As mixing time increased, the solution turned from orange (i.e., the typical color of a PTMSDPA/toluene solution) to dark red, which is the color of PDPA reported by Teraguchi and Masuda.²⁰ When a PTMSDPA/MgO solution was allowed to mix for extended periods

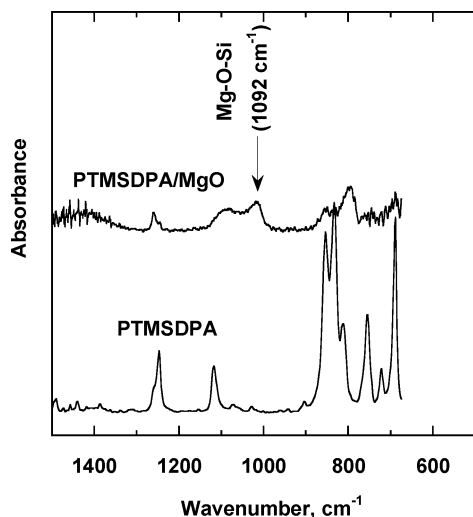


Figure 5. ATR FTIR spectra of PTMSDPA and PTMSDPA containing 0.2 volume fraction MgO. The spectrum of PTMSDPA/MgO was shifted vertically for easier viewing.

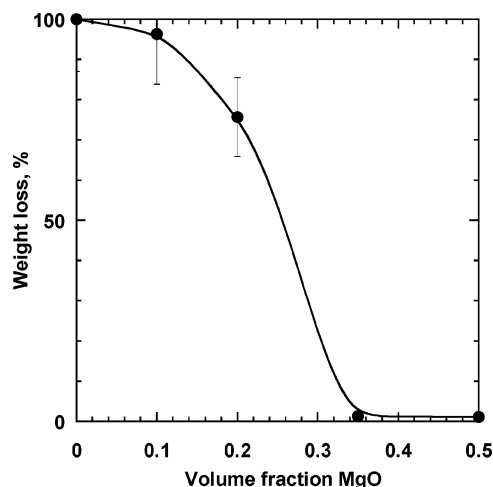


Figure 6. Influence of MgO nanoparticle content in PTMSDPA on weight loss after extraction in toluene for 2 weeks, as calculated by eq 6. Solutions were mixed for 5 days at $-10\text{ }^{\circ}\text{C}$. The uncertainty in sample weight after toluene extraction is indicated by the error bars on the data points, and they represent the standard deviation from multiple experiments. The volume fraction MgO corresponds to the particle content in the polymer films prior to the start of the extraction study.

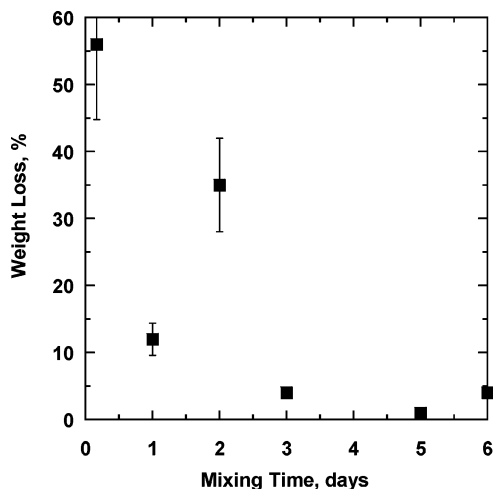


Figure 7. Influence of mixing time on PTMSDPA/MgO film weight loss after extracting in toluene for 2 weeks, as calculated using eq 6. Samples were mixed at $23\text{ }^{\circ}\text{C}$, and the film before extraction contained 0.2 volume fraction MgO. The uncertainty in sample weight after toluene extraction is indicated by the error bars on the data points, and they represent the standard deviation from multiple experiments.

of time (e.g., 6 days at room temperature), it would gel. This observation is another qualitative indication consistent with the formation of toluene-insoluble PDPA in the presence of MgO nanoparticles.

The effect of temperature on desilylation was similar to that of mixing time and MgO loading. Increasing the mixing temperature decreased the weight loss of PTMSDPA/MgO samples after toluene extraction. After 5 days of mixing the solution at $-10\text{ }^{\circ}\text{C}$, there was substantial weight loss (i.e., 76%), whereas at higher solution mixing temperatures, PTMSDPA/MgO films were essentially insoluble in toluene and experienced practically no detectable weight loss (i.e., weight loss was 2% at $0\text{ }^{\circ}\text{C}$ and 4% at $23\text{ }^{\circ}\text{C}$). Presumably, the reaction between the particles and polymer was favored at higher temperatures. Therefore, at a fixed mixing time, the extent of reaction, as characterized by weight loss upon extraction in toluene, was higher at higher temperatures.

Table 3. Permeability of MgO-Filled PTMSDPA Films Mixed at -10°C for 5 Days^a

MgO vol fraction	CO ₂ permeability, kbarrer	CH ₄ permeability, kbarrer	$\alpha_{\text{CO}_2/\text{CH}_4}$
0	6.0 \pm 0.6	2.7 \pm 0.3	2.2 \pm 0.2
0.1	6.0 \pm 0.6	3.8 \pm 0.4	1.6 \pm 0.2
0.25	8.6 \pm 0.8	5.3 \pm 0.5	1.6 \pm 0.2
0.5	40 \pm 4	19 \pm 1.9	2.2 \pm 0.2

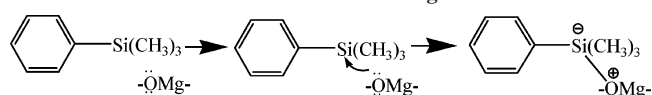
^a Experiments were conducted at 35°C and $\Delta p = 3.4$ atm. Permeability is expressed in kbarrer (kilobarrer), where 1 kbarrer = 10^{-7} cm³(STP)/cm/(cm² s cmHg).

Table 3 presents pure gas CO₂ and CH₄ permeability in filled PTMSDPA. The gas permeability generally increases with increasing particle loading. At 0.1 volume fraction MgO, CO₂ permeability was similar to that of PTMSDPA, (i.e., 6 kbarrer), which is somewhat higher than the CO₂ permeability in PTMSDPA reported by Raharjo et al. (i.e., 4 kbarrer).²¹ The difference between the unfilled PTMSDPA permeability reported here and that reported by Raharjo et al. may be attributed to differences in sample processing history.²¹ However, at 0.1 volume fraction MgO, CH₄ permeability is higher than that of the particle-free polymer. At MgO loadings greater than 0.1 volume fraction, the permeability of both gases increased. The nanocomposite film with 0.5 volume fraction MgO exhibited a CO₂ permeability of 40.3 kbarrer and a CO₂/CH₄ selectivity of 2.2. The CO₂ permeability of the 0.5 volume fraction filled PTMSDPA is ~ 25 times higher than the CO₂ permeability reported for PDPA (i.e., 1.5 kbarrer)²¹ and over 6 times higher than that for PTMSDPA, whereas the CO₂/CH₄ selectivity is somewhat lower than the CO₂/CH₄ selectivity values reported by Raharjo et al. for PDPA and PTMSDPA, which were 3.3 for both materials.²¹

Particle Dispersion. Atomic force microscopy and transmission electron microscopy were used to characterize the nanoparticle dispersion in the polymers, and the results from this study will be reported elsewhere.⁵¹ In general, the particles disperse into agglomerates of characteristic dimensions on the order of tens of nanometers at low nanoparticle loadings, (i.e., less than 0.1 volume fraction MgO). At these loadings, some nanoparticles form larger agglomerates, (i.e., agglomerate characteristic dimensions of 100–1000 nm). However, such large agglomerates are rare for nanoparticle loadings below 0.1 volume fraction. As nanoparticle loading increases, the size and concentration of larger particle agglomerates increase.

Desilylation of Model Compounds. One obstacle encountered in the study of PTMSDPA desilylation is that the resulting product, PDPA, is insoluble, which limits structural characterization of the resulting desilylated compound. To provide further evidence of this reaction and to study it in more detail, low molar mass model compounds (cf. Table 2) containing a TMS unit connected to an aromatic ring (trimethyl(phenyl)silane (TMPS)) or via an ethylene linkage, (1-phenyl-2-(trimethylsilyl)-ethylene (PhTMSE)), or an acetylene linkage (1-phenyl-2-(trimethylsilyl)acetylene (PhTMSA)), were selected to study desilylation in the presence of MgO nanoparticles. Since these are low molar mass compounds, they remain soluble even after reaction with the particles, which enables characterization via NMR.

Treating TMPS with MgO does not transfer the TMS group as discussed with PTMSP and PTMSDPA, but MgO treatment results in an interaction between the nanoparticles and the small molecule, as proposed in Scheme 7. Proton and ¹³C NMR did not show any reaction products for MgO-treated TMPS. Any material bound to a nanoparticle (i.e., any TMPS molecule

Scheme 7. Interaction between MgO and TMPS

whose silicon atom has a p–d bond with the nanoparticle) would not be in solution since the MgO particles are not soluble in d-benzene. However, a chalky residue formed on the side of the mixing vessel during treatment was presumed to be MgO-treated TMPS. The FTIR spectrum of the chalky material (cf. Figure 8) shows peaks at 1160 and 1090 cm⁻¹ that are not present in the neat TMPS. The chalky residue (i.e., MgO-treated TMPS) also has a peak that is shifted relative to that of untreated TMPS. The new peak at 1160 cm⁻¹ is attributed to the in-plane CH bending vibrations of monosubstituted benzene.⁴⁵ This vibration is more pronounced in the MgO-treated TMPS than in untreated TMPS, which might indicate a change in the monosubstituted benzene, such as the formation of a p–d bond between Si and the nanoparticle oxygen lone pair electrons. The peak at 1090 cm⁻¹ is attributed to Si–O bonds.^{45,52} The broadly shifted peak between 1200 and 1275 cm⁻¹ in the chalky residue spectrum is ascribed to the SiC–H,^{19,45} and it is consistent with FTIR spectra of other molecules containing TMS groups or phenyl–silicon bonds where the silicon atom is bound to substituents of varying chemistry (i.e., alcohols, amines, halogens, etc.).⁴⁵

¹H NMR revealed several new peaks in the MgO-treated PhTMSE spectrum that were not present in the untreated PhTMSE spectrum. The TMS peaks (i.e., peaks near 0 ppm) were not changed upon treatment with MgO. A reaction is believed to occur between PhTMSE and the MgO particles which does not involve the TMS group. Therefore, PhTMSE was not a good model compound for the study of the MgO nanoparticle induced desilylation reaction, and studies of this compound were discontinued.

The acetylene group in PhTMSA did not react with MgO. The aromatic group of PhTMSA mimics, albeit crudely,

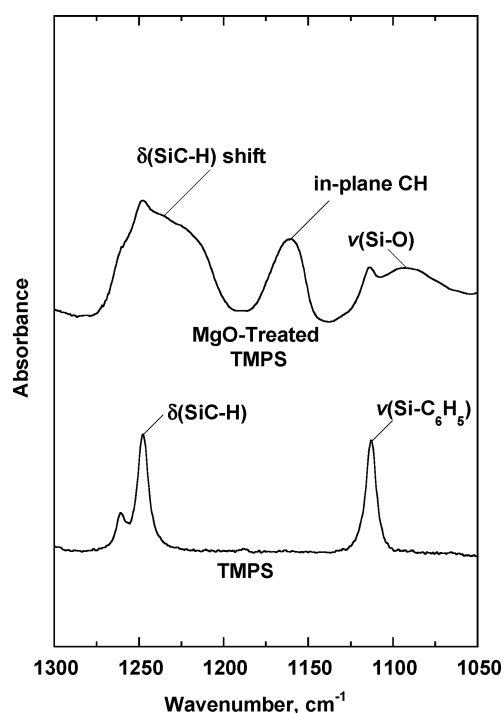
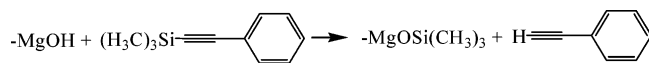


Figure 8. FTIR transmission spectra of TMPS and MgO-treated TMPS in KBr pellets. The spectra have been shifted vertically for easier viewing.

Scheme 8. MgO-Induced PhTMSA Desilylation Reaction



conjugation of the PTMSDPA phenyl rings and also stabilizes oxygen–silicon p–d bonds.²⁴ To be consistent with the reaction mechanism proposed in the literature for basic alcohol groups reacting with TMS-containing compounds (i.e., Scheme 3), the desilylation reaction of PhTMSA would follow Scheme 8. Figure 9 presents the FTIR spectrum of PhTMSA and the spectrum of MgO-treated PhTMSA with a TMS content of 0.08 mol of TMS/g of MgO, which is equivalent to the TMS/MgO ratio for a PTMSP film containing 0.2 volume fraction MgO. There is a broad peak in the MgO-treated PhTMSA spectrum at 1107 cm⁻¹, which is not present in the spectrum of PhTMSA. This peak is consistent with the presence of Si–O bonds,⁴⁵ and it is ascribed to –Mg–O–Si bonds.

As shown in Figure 10a, the PhTMSA ¹H NMR spectrum exhibited peaks at 7.4, 6.8, and 0.3 ppm, which are attributed to the para hydrogen, meta and ortho hydrogens, and the TMS hydrogen, respectively. These peaks are consistent with those reported in the literature.⁵³ The peak at 7.2 ppm is attributed to the hydrogen atoms on the d-benzene solvent. As shown in Figure 10b, relative to PhTMSA, there were three new peaks in the ¹H NMR spectrum of MgO-treated PhTMSA (TMS/MgO ratio = 0.08 mol/g) at 7.39, 2.72, and 0.10 ppm. The peak at 7.39 ppm (g, h) corresponds to the *m*-phenyl protons on desilylated PhTMSA samples.⁵⁴ The peak at 2.72 ppm (e) is assigned to the proton bound to the acetylene unit,⁵⁴ confirming the hydrogen–TMS transfer between –MgOH and PhTMSA. Peak i has a chemical shift slightly lower than that of the TMS proton peak in PhTMSA, i.e., peak a; therefore, peak i is ascribed to the TMS protons in –OTMS. The –OTMS/acetylene proton integral ratio (i.e., the ratios of the peaks at 0.20 and 0.10 ppm) is 9:1, which is the stoichiometric ratio required by the proposed reaction (cf. Scheme 8).

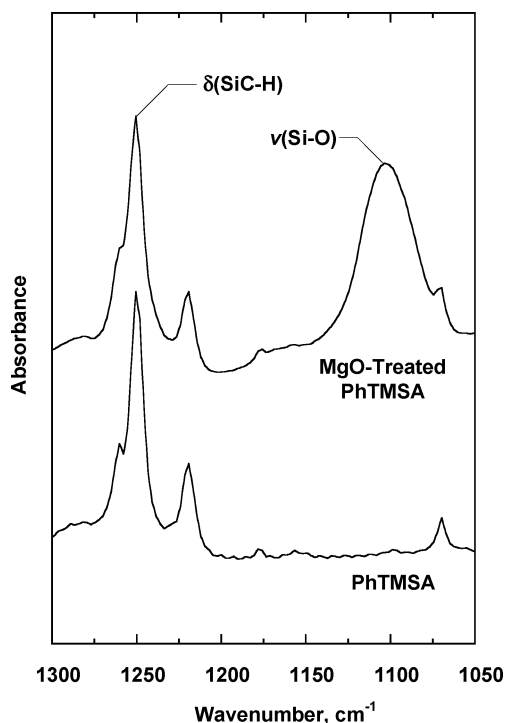


Figure 9. FTIR transmission spectra of PhTMSA and MgO-treated PhTMSA in KBr pellets. The spectra have been shifted vertically for easier viewing.

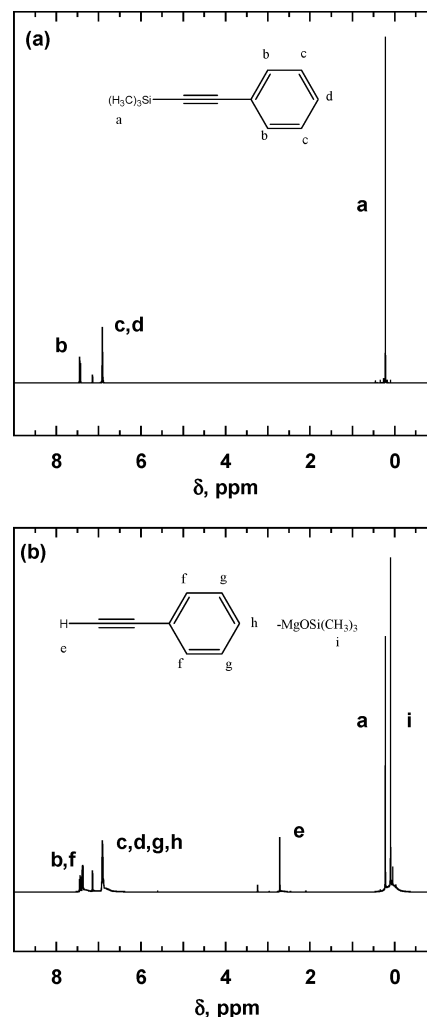


Figure 10. ¹H NMR spectrum of (a) PhTMSA and (b) MgO-treated PhTMSA.

Using the NMR data in Figure 10, the fractional desilylation, X_{TMS} (percentage of moles of TMS removed/total moles of TMS), was characterized by two methods. First, if the TMS groups are conserved, a TMS balance of the proton integral values of peaks a and i yields the following estimate:

$$X_{\text{TMS}} = \frac{I_i}{I_i + I_a} \times 100 \quad (9)$$

where I_i and I_a are the proton integral values for peak i (the TMS group of –OTMS) and peak a (the TMS group of PhTMSA), respectively. The second method involves comparing the integral of peak a, the TMS group of PhTMSA, to that of the desilylated PhTMSA proton peak e:

$$X_{\text{TMS}} = \frac{I_e}{I_e + \frac{I_a}{9}} \times 100 \quad (10)$$

where I_e is the proton integral value of the desilylated PhTMSA proton peak e. In this case, I_a is divided by nine because there are nine hydrogen atoms on a TMS group, and they are replaced by one hydrogen when desilylation occurs. Equation 10 is generally the better method of calculating X_{TMS} since the –OTMS peak does not always appear in solution-state NMR spectrum in samples where the nanoparticles could not be adequately dispersed in d-benzene to be detected. The fractional

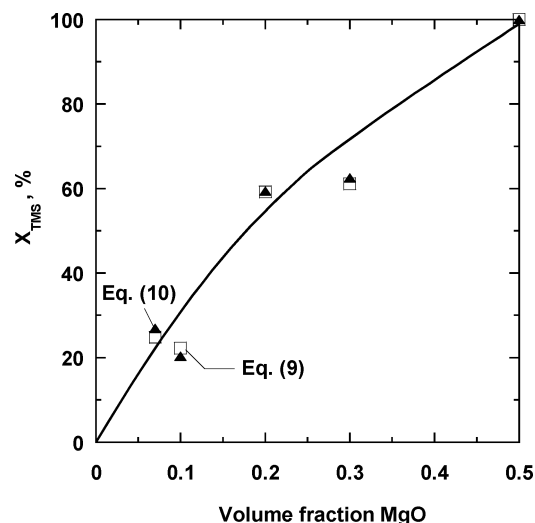


Figure 11. Influence of MgO content on estimated percentage desilylation of PhTMSA, X_{TMS} , as calculated by eq 9 and estimated percentage of trimethylsilyl groups on the MgO particles as calculated by eq 10.

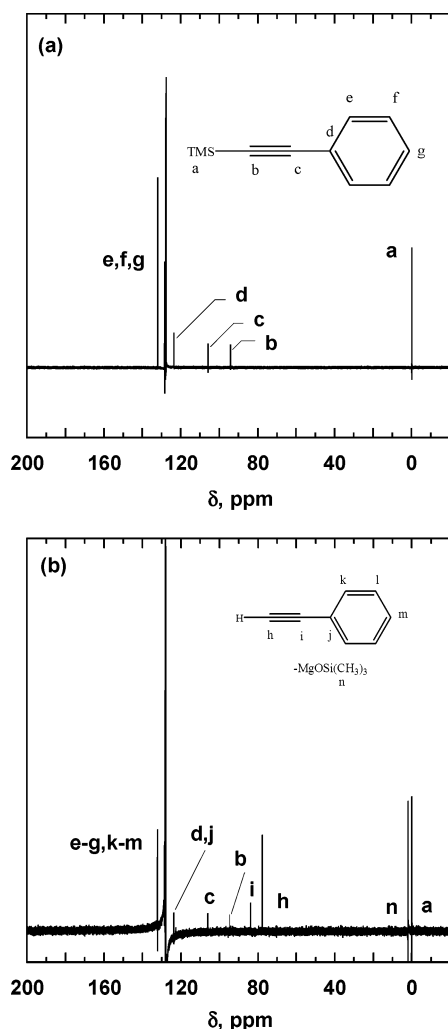


Figure 12. ^{13}C NMR spectrum of (a) PhTMSA and (b) MgO-treated PhTMSA.

desilylation of MgO-treated PhTMSA based upon eqs 9 and 10 yield similar results, as shown in Figure 11. Both methods indicated an increase in fractional desilylation with increasing particle loading and essentially complete desilylation (i.e., X_{TMS}

= 100%) of PhTMSA at a volume fraction of MgO equal to 0.5.

The ^{13}C NMR spectrum revealed a chemical change when PhTMSA was contacted with MgO (cf. Figure 12a,b). As shown in Figure 12a, PhTMSA peaks at 106 ppm (c) and 94 ppm (b) represent the acetylene carbons, while the peak at 0 ppm (a) corresponds to the TMS carbons,⁵⁴ and it is consistent with the ^{13}C NMR spectrum reported in the literature.⁵³ As shown in Figure 12b, three new peaks appeared for the MgO-treated PhTMSA at 84, 78, and 2 ppm. The peaks at 84 ppm (i) and 78 ppm (h) represent desilylated acetylene carbons.⁵⁴ The peak at 2 ppm (n) is attributed to $-\text{OTMS}$ since the chemical shift is near 0, as expected for a TMS group, yet it is not equivalent to the TMS chemical shift observed for untreated PhTMSA. In this case, the $-\text{OTMS}$ peak is present due to its high concentration in the solution (60 mol % based on eq 9).

Conclusions

In much of the literature on polymer nanocomposites for gas separation applications, nanoparticles are presumed to be chemically inert toward the polymer. However, this assumption is not obeyed by metal oxides such as MgO in materials such as those considered in this study. The reaction and permeation data demonstrate that metal oxide nanoparticles can alter the chemical properties and enhance the gas transport properties of polymeric membranes. The desilylation reaction between TMS-bearing compounds and MgO nanoparticles was substantiated via model compound studies. The chemical stability and gas permeability of the polymers increase with increasing particle loading. At high MgO loadings (i.e., 0.5 volume fraction), the nanocomposite films are insoluble in common solvents and exhibit CO_2 permeability coefficients nearly 1 order of magnitude greater than that of the native polymer. Although this is only one example of nanoparticle-treated polymeric membranes, the technique of adding nanoparticles that react with the polymer matrix presents one relatively unexplored route to prepare membrane materials with enhanced gas transport properties and improved chemical stability. So far, it is not known to what extent particle size affects these results and whether other particles might behave similarly.

Acknowledgment. We gratefully acknowledge partial support of this work by the U.S. Department of Energy (Grant DE-FG02-02ER15362).

References and Notes

- (1) Baker, R. W. *Ind. Eng. Chem. Res.* **2002**, *41*, 1393–1411.
- (2) Baker, R. W. *Membrane Technology and Applications*, 2nd ed.; McGraw-Hill: New York, 2004.
- (3) Freeman, B. D.; Pinnau, I. *Trends Polym. Sci.* **1997**, *5*, 167–173.
- (4) Matteucci, S. T.; Yampol'skii, Y. P.; Freeman, B. D.; Pinnau, I. Transport of gases and vapors in glassy and rubbery polymers. In *Materials Science of Membranes for Gas and Vapor Separations*; Yampol'skii, Y. P., Freeman, B. D., Pinnau, I., Eds.; John Wiley and Sons: London, 2006; pp 1–48.
- (5) Nagai, K.; Masuda, T.; Nakagawa, T.; Freeman, B. D.; Pinnau, I. *Prog. Polym. Sci.* **2001**, *26*, 721–798.
- (6) Merkel, T. C.; He, Z.; Pinnau, I.; Freeman, B. D.; Hill, A. J.; Meakin, P. *Macromolecules* **2003**, *36*, 8406–8414.
- (7) Toy, L. G.; Nagai, K.; Freeman, B. D.; Pinnau, I.; He, Z.; Masuda, T.; Teraguchi, M.; Yampolskii, Y. P. *Macromolecules* **2000**, *22*, 2516–2524.
- (8) Merkel, T. C.; Freeman, B. D.; Spontak, R. J.; He, Z.; Pinnau, I.; Meakin, P.; Hill, A. J. *Science* **2002**, *296*, 519–522.
- (9) Merkel, T. C.; Freeman, B. D.; Spontak, R. J.; He, Z.; Pinnau, I.; Meakin, P.; Hill, A. J. *Chem. Mater.* **2003**, *15*, 109–123.
- (10) He, Z.; Pinnau, I.; Morisato, A. *Desalination* **2002**, *146*, 11–15.

- (11) Teplyakov, V. V.; Roizard, D.; Farve, E.; Khotimsky, V. S. *J. Membr. Sci.* **2003**, *220*, 165–175.
- (12) Pinnau, I.; Toy, L. G. *J. Membr. Sci.* **1996**, *116*, 199–209.
- (13) White, L. S.; Blinka, T. A.; Kloczewski, H. A.; Wang, I. *J. Membr. Sci.* **1995**, *103*, 73–82.
- (14) Ratcliffe, C. T.; Diaz, A.; Nopasit, C.; Munoz, G. In *Laurence Reid Gas Conditioning Conference*; Norman, OK, 1999; pp 118–140.
- (15) Masuda, T.; Isobe, E.; Higashimura, T. *Macromolecules* **1985**, *18*, 841–845.
- (16) Tsuchihara, K.; Masuda, T.; Higashimura, T. *Macromolecules* **1992**, *25*, 5816–5820.
- (17) Chien, J. C. W.; Wnek, G. E.; Karasz, F. E.; Hirsch, J. A. *Macromolecules* **1981**, *14*, 479–485.
- (18) Niki, A.; Masuda, T.; Higashimura, T. *J. Polym. Sci., Part A: Polym. Chem.* **1987**, *25*, 1553–1562.
- (19) Sakaguchi, T.; Yumoto, K.; Shiotsuki, M.; Sanda, F.; Yoshikawa, M.; Masuda, T. *Macromolecules* **2005**, *38*, 2704–2709.
- (20) Teraguchi, M.; Masuda, T. *Macromolecules* **2002**, *35*, 1149–1151.
- (21) Raharjo, R. D.; Lee, H. J.; Freeman, B. D.; Sakaguchi, T.; Masuda, T. *Polymer* **2005**, *46*, 6316–6324.
- (22) Teplyakov, V. V.; Durgaryan, S. G. *Vysokomol. Soedin., A* **1984**, *26*, 1498–1505.
- (23) Teplyakov, V. V.; Meares, P. *Gas Sep. Purif.* **1990**, *4*, 66–73.
- (24) Pierce, A. E. *Silylation of Organic Compounds*; Pierce Chemical Co.: Rockford, IL, 1968.
- (25) Sommer, L. H. *Stereochemistry, Mechanism, and Silicon*; McGraw Hill: New York, 1965.
- (26) Henglein, F. A.; Scheinost, K. *Makromol. Chem.* **1956**, *21*, 59–73.
- (27) Ghosal, K.; Freeman, B. D. *Polym. Adv. Technol.* **1994**, *5*, 673–697.
- (28) Freeman, B. D.; Pinnau, I. *Polymeric materials for gas separations*. In *Polymer Membranes for Gas and Vapor Separation*; ACS Symposium Series Vol. 733; Freeman, B. D., Pinnau, I., Eds.; American Chemical Society: Washington, DC, 1999; pp 1–27.
- (29) Vu, D. Q.; Koros, W. J.; Miller, S. J. *J. Membr. Sci.* **2003**, *211*, 335–348.
- (30) Bouma, R. H. B.; Checchetti, A.; Chidichimo, G.; Drioli, E. *J. Membr. Sci.* **1997**, *128*, 141–149.
- (31) Barrer, R. M.; Barrie, J. A.; Rogers, M. G. *J. Polym. Sci., Part A: Polym. Chem.* **1963**, *1*, 2565–2586.
- (32) Merkel, T. C.; Freeman, B. D.; Spontak, R. J.; He, Z.; Pinnau, I.; Hill, A. J. *Chem. Mater.* **2003**, *15*, 109–123.
- (33) Koper, O. B.; Lagadic, I.; Volodin, A. M.; Klabunde, K. J. *Chem. Mater.* **1997**, *9*, 2468–2480.
- (34) Matteucci, S. T.; Kusuma, V.; Sanders, D.; Freeman, B. D. Manuscript in preparation.
- (35) Utamapanya, S.; Klabunde, K. J.; Schlup, J. R. *Chem. Mater.* **1991**, *3*, 175–181.
- (36) Stern, S. A.; Gareis, P. J.; Sinclair, T. F.; Mohr, P. H. *J. Appl. Polym. Sci.* **1963**, *7*, 2035–2051.
- (37) Merkel, T. C.; Bondar, V.; Nagai, K.; Freeman, B. D. *J. Polym. Sci., Part B: Polym. Phys.* **2000**, *38*, 273–296.
- (38) Yu, Y.; Guo, Q.; Liu, S.; Wang, E. *Phys. Rev. B* **2003**, *68*, 1–4.
- (39) Rollason, R. J.; Plane, J. M. C. *Phys. Chem. Chem. Phys.* **2001**, *3*, 4733–4740.
- (40) Wang, J. A.; Novaro, O.; Bokhimi, X.; Lopez, T.; Gomez, R.; Navarrete, J.; Llanos, M. E.; Lopez-Salinas, E. *J. Phys. Chem. B* **1997**, *101*, 7448–7451.
- (41) Atteya, M.; Klabunde, K. J. *Chem. Mater.* **1991**, *3*, 182–187.
- (42) Gerstein, M.; Tsai, J.; Levitt, M. *J. Mol. Biol.* **1995**, *249*, 955–966.
- (43) Mekhemer, G. A. H.; Halaway, S. A.; Mohamed, M. A.; Zaki, M. I. *J. Phys. Chem. B* **2004**, *108*, 13379–13386.
- (44) Rethwisch, D. G.; Dumesic, J. A. *Langmuir* **1986**, *2*, 73–79.
- (45) Colthup, N. B.; Daly, L. H.; Wiberly, S. E. *Introduction to Infrared and Raman Spectroscopy*, 2nd ed.; Academic Press: New York, 1975.
- (46) Gregg, S.; Ramsay, J. D. *J. Chem. Soc. A* **1970**, 2784–2787.
- (47) Sherrill, A. B.; Barteau, M. A. *J. Mol. Catal. A: Chem.* **2002**, *184*, 301–310.
- (48) Paparazzo, E.; Fanfoni, M.; Severini, E. *Appl. Surf. Sci.* **1992**, *56–58*, 866–872.
- (49) Leclerc, M.; Prud'homme, R. E.; Soum, A.; Fontanille, M. *J. Polym. Sci., Part B: Polym. Phys.* **1985**, *23*, 2031–2041.
- (50) Sone, T.; Asako, R.; Masuda, T.; Tabata, M.; Wada, T.; Sasabe, H. *Macromolecules* **2001**, *34*, 1586–1592.
- (51) Matteucci, S. T.; Kusuma, V.; Freeman, B. D. Manuscript in preparation.
- (52) Helmy, R.; Wenslow, R. W.; Fadeev, A. Y. *J. Am. Chem. Soc.* **2004**, *126*, 7595–7600.
- (53) Bartik, T.; Happ, B.; Iglewsky, M.; Bandmann, H.; Boese, R.; Helmbach, P.; Hoffmann, T.; Wenschuh, E. *Organometallics* **1992**, *11*, 1235–1241.
- (54) Silverstein, R. M.; Webster, F. X. *Spectrometric Identification of Organic Compounds*, 6th ed.; John Wiley & Sons: New York, 1998.

MA062421S